7. Baan, W. A. Infrared properties of OH galaxies. *Astrophys. J.* **338,** 804–811 (1989).
8. Graham, J. R. *et al.* The double nucleus of Arp 330 unveiled. *Astrophys. J.* **354,** L5–L8 (1990).
9. Baan, W. A. & Haschick, A. D. Nuclear antics of IC 4553 (Arp 220). *Astrophys. J.* **454,** 745–748 (1995).
10. Diamond, P. J., Norris, R. P., Baan, W. A. & Booth, R. S. VLBI observations of the OH megamaser in IC 4553 (Arp 220). *Astrophys. J.* **340,** L49–L52 (1989).
11. Lonsdale, C. J., Diamond, P. J., Smith, H. E. & Lonsdale, C. J. Compact OH megamaser and probable quasar activity in the galaxy Arp 220. *Nature* **370,** 117–120 (1994).
12. Goldreich, P., Scoville, N. OH/IR Stars I—Physical properties of circumstellar envelopes. *Astrophys. J.* **205,** 144–154 (1976).
13. Savage, B. D. & Mathis, J. S. Observed properties of interstellar dust. *Annu. Rev. Astron. Astrophys.* **17,** 73–111 (1979).
14. Sturm, E. *et al.* ISO-SWS spectroscopy of Arp 220: a highly obscured starburst galaxy. *Astron. Astrophys.* **315,** L133–L136 (1996).
15. Lutz, D. *et al.* What powers luminous infrared galaxies? *Astron. Astrophys.* **315,** L137–L140 (1996).
16. Destombes, J. L., Marliere, C., Baudry, A. & Brillet, J. The exact hyperfine structure and Einstein A-coefficients of OH—consequences in simple astrophysical models. *Astron. Astrophys.* **60,** 55–60 (1977).

Acknowledgements. This work is based on observations with ISO, an ESA project with instruments funded by the ESA Member States (especially the PI countries: France, Germany, the Netherlands and the UK) and with the participation of ISAS and NASA.

Correspondence and requests for materials should be addressed to C.J.S. (e-mail: skinner@stsci.edu).

Individual single-wall carbon nanotubes as quantum wires

Sander J. Tans*, Michel H. Devoret*†, Hongjie Dai‡, Andreas Thess‡, Richard E. Smalley‡, L. J. Geerligs* & Cees Dekker*

* *Department of Applied Physics and DIMES, Delft University of Technology, Lorentzweg 1, 2628 CJ Delft, The Netherlands*
‡ *Center for Nanoscale Science and Technology, Rice Quantum Institute, and Departments of Chemistry and Physics, MS-100, Rice University, PO Box 1892, Houston, Texas 77251, USA*

Carbon nanotubes have been regarded since their discovery[1] as potential molecular quantum wires. In the case of multi-wall nanotubes, where many tubes are arranged in a coaxial fashion, the electrical properties of individual tubes have been shown to vary strongly from tube to tube[2,3], and to be characterized by disorder and localization[4]. Single-wall nanotubes[5,6] (SWNTs) have recently been obtained with high yields and structural uniformity[7]. Particular varieties of these highly symmetric structures have been predicted to be metallic, with electrical conduction occurring through only two electronic modes[8–10]. Because of the structural symmetry and stiffness of SWNTs, their molecular wavefunctions may extend over the entire tube. Here we report electrical transport measurements on individual single-wall nanotubes that confirm these theoretical predictions. We find that SWNTs indeed act as genuine quantum wires. Electrical conduction seems to occur through well separated, discrete electron states that are quantum-mechanically coherent over long distance, that is at least from contact to contact (140 nm). Data in a magnetic field indicate shifting of these states due to the Zeeman effect.

The electronic band structure of carbon nanotubes presents some peculiar features. Owing to the hexagonal symmetry of a graphene sheet, the Fermi contour expected for a two-dimensional lattice reduces to six points[11]. In a nanotube, the component of momentum along the circumference of the tube will be quantized owing to periodic boundary conditions. For so-called 'armchair' SWNTs (see ref. 12 for an overview), this results in only two one-dimensional gapless modes of propagation parallel to the tube axis[8–10]. In the simplest approach, we consider the electron states to be four-fold degenerate, including spin. The strictly one-dimensional nature of the modes implies that the angular momentum contribution to the magnetic energy is zero. The magnetic energy is expected to be dominated by the spin contribution $g\mu_B B$ (Zeeman energy), where μ_B is the Bohr magneton, g is the Landé g-factor, and B the magnetic field. For a finite one-dimensional tube of length L, the component of momentum along the axis will also be quantized. This results in 'particle-in-a-box' energy separation between levels of $\Delta E = hv_F/2L$. From band-structure calculations[11], we can find an estimate for the Fermi velocity $v_F \approx 8.1 \times 10^5\ \mathrm{m\,s^{-1}}$. Even a 3-μm-long tube would thus have a considerable splitting energy of $\Delta E \approx 0.6$ meV.

The nanotubes are produced by laser-vaporization of carbon with an admixture of Ni/Co, as described elsewhere[7]. This technique results in samples enriched in armchair SWNTs with a uniform diameter of 1.38 nm. After deposition on the Si/SiO_2 substrate, the tubes are imaged by an atomic force microscope (AFM). The images show tubular features with lengths of the order of micrometres and heights between ~1 and ~50 nm. The 1-nm-high features are identified as individual single-wall tubes. Discrepancy of this value with the assumed diameter of 1.38 nm is believed to come from plastic deformation of the tube resulting from tip–sample forces. The larger features in the images are ropes of parallel tubes[7]. Figure 1 shows an AFM image of an individual tube connected to two electrodes and a corresponding circuit diagram. The two-point resistance at room-temperature of single-tube samples generally is ~1 MΩ, and appears to scale with the overlap area with the electrode. (The resistance at room temperature is 550 kΩ for the sample in Fig. 1.) On a different single-tube sample with a four-point geometry, we determined the contact resistance to be around 300 kΩ at room temperature and 1 MΩ at 4 K. The measurements presented here were performed on the sample displayed in Fig. 1 in a dilution refrigerator with a mixing-chamber base temperature of 5 mK. Three other samples yielded similar results.

Typical current–voltage curves at various gate voltages are shown in Fig. 2a. Around zero bias voltage a clear gap is present. For higher voltages, the current increases in steps. The gap appears to be suppressed for certain gate voltages and has a maximum value in between (see inset). In Fig. 2b, the current is shown as a function of the gate voltage at bias voltage $V_{bias} = 30\ \mu V$. The sequence of current peaks indicates that the suppression of the gap occurs in a

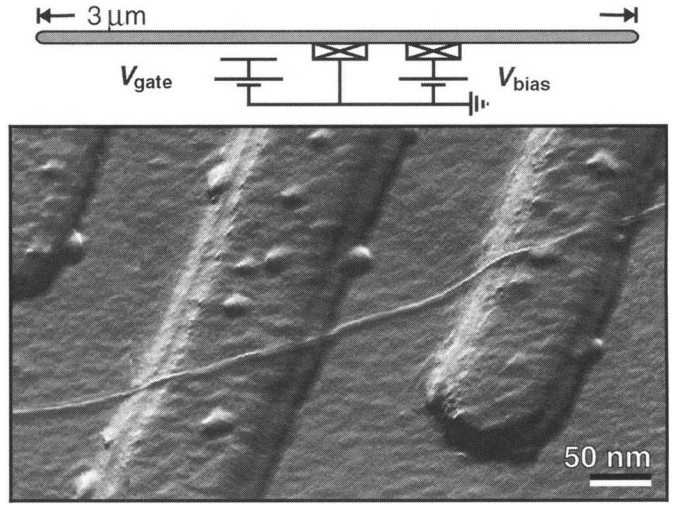

Figure 1 AFM tapping-mode image of a carbon nanotube on top of a Si/SiO_2 substrate with two 15-nm-thick Pt electrodes, and a corresponding circuit diagram. The nanotubes are deposited by spin-coating of a drop of nanotube suspension. This tube has a diameter of ~1 nm, as deduced from AFM height profiles, and is identified as an individual single-wall nanotube. The total length of the tube is 3 μm, with a section of 140 nm between the contacts to which a bias voltage V_{bias} is applied. A gate voltage V_{gate} applied to the third electrode in the upper-left corner of the image is used to vary the electrostatic potential of the tube.

† Permanent address: Service de Physique de l'Etat Condensé, CEA-Saclay, F-91191 Gif-sur-Yvette, France.

quasi-periodic fashion. The same pattern of peaks persists up to very large scans of gate voltage V_{gate} (at least from -2.5 to $+2.5$ V). The observations indicate Coulomb charging[13] of the nanotube. Coulomb charging occurs when the contact resistance is larger than the quantum resistance R_K ($R_K = h/e^2 \approx 26\,k\Omega$) and when the total capacitance C of the object is so small that adding a single electron costs a significant charging energy $E_c = e^2/2C$. At low temperatures, that is, $k_B T \ll E_c$, the current is thus blocked and will flow only when $V_{bias} > e/2C$. However, zero-bias conductance can be restored by precisely 'tuning' the electrostatic potential of the tube with the gate voltage. The two traces in Fig. 2b were taken under identical conditions and show an occasional doubling of certain peaks. This bistability may be the result of switching offset charges[13] that shift the potential of the tube. We have concentrated measurements on peaks that do not show this bistability.

In Fig. 3 we show measurements of a single conductance peak at $V_{bias} = 10\,\mu V$. The height of the conductance peak in Fig. 3 appears to decrease strongly with increasing temperature. This is a signature of resonant tunnelling through a discrete electron level that is aligned with the Fermi energy E_F of the electrodes (see left inset)[14]. We label this level as gg (ground state to ground state) because when it alternates in time between being unoccupied and occupied, the tube is in the ground state in both cases. This gg-orbital is well separated by an energy ΔE from the occupied orbital below, and by $\Delta E'$ from the unoccupied orbital above. The conductance through the gg-orbital is now only dependent on the difference in electron occupancy at E_F between the two contacts which, at resonance, goes down with increasing temperature. If the density of states in the tube were continuous, the conductance maximum would be constant with increasing temperature[14]. The resonant tunnelling through discrete electron levels implies that single molecular orbitals carry the current, and accordingly are phase coherent and extended over a distance of at least 140 nm (the distance between the electrodes). This is a crucial observation. It shows that the electrons are not strongly localized despite the

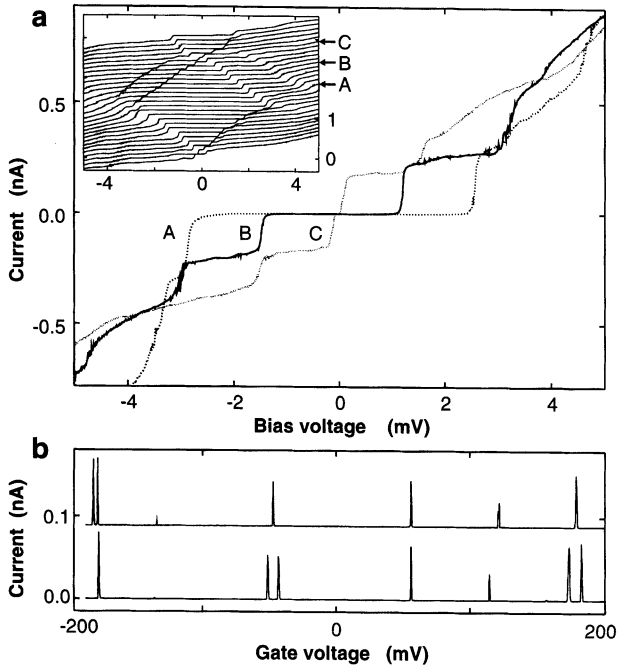

Figure 2 a, Current–voltage curves of the nanotube at a gate voltage of 88.2 mV (trace A), 104.1 mV (trace B) and 120.0 mV (trace C). Inset, more I–V_{bias} curves with V_{gate} ranging from 50 mV (bottom curve) to 136 mV (top curve), with vertical offsets for clarity. The variation with V_{gate} of the gap around zero bias voltage implies Coulomb charging of the tube. The stepwise increase of the current at higher voltages may result from an increasing number of excited states entering in the bias window. **b**, Current versus gate voltage at $V_{bias} = 30\,\mu V$. Two traces are shown that were performed under the same conditions.

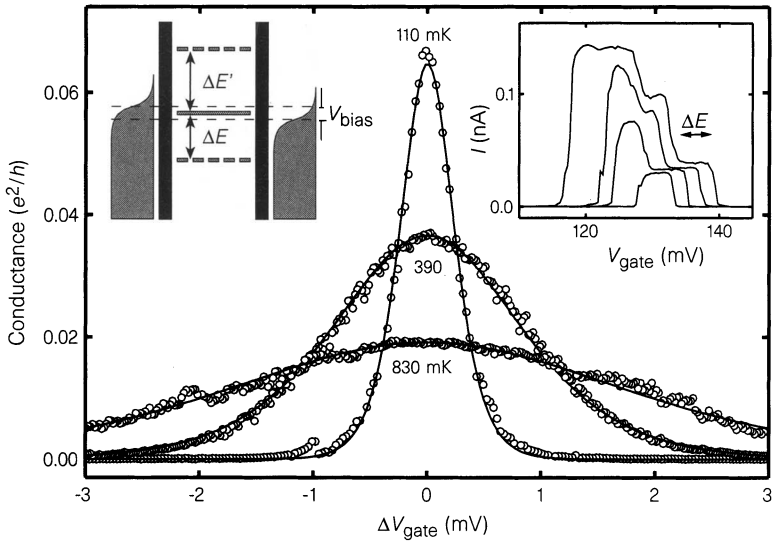

Figure 3 Conductance $G = I/V_{bias}$ versus ΔV_{gate} at low bias voltage $V_{bias} = 10\,\mu V$ and different temperatures. Solid lines are fits of $G \propto \cosh^{-2}(e\Delta V_{gate}/\alpha 2k_B T)$, corresponding to the model of a single molecular level that is weakly coupled to two electrodes[14] (see inset). The factor α converts ΔV_{gate} into the corresponding electrostatic potential shift of the tube. For this peak $\alpha = 16$. The solid bar in the left inset denotes the gg-level (see text) and is well separated by energies ΔE, $\Delta E' \gg k_B T$ from the eg (lower broken bar) and ge (upper broken bar) levels that involve excited states of the tube. At a certain gate voltage, the gg-level will be in the bias window, resulting in resonant tunnelling of electrons. ΔV_{gate} is the gate voltage taken relative to V_{gate} at resonance. The indicated temperatures result from fits of this model. The corresponding thermometer temperatures are 5, 240 and 600 mK, respectively. The discrepancy between the two temperatures can be attributed to additional broadening due to the finite bias voltage ($10\,\mu V \equiv 116$ mK) and residual noise in the measurement system. From the maximum of the peak we obtain a lower bound on electronic transmission of 1/60, which includes the contact resistance. In the right inset we plot the current as a function of V_{gate} for higher $V_{bias} = 0.4$, 0.8, 1.2 and 1.6 mV. For this peak, $\alpha = 12$. The steps in the peak are a result of lower-lying levels in the bias window.

one-dimensional nature of the tube and potentially perturbing influences like structural imperfections, bends and twists of the tube, and charge defects in the SiO_2 support. Apparently the structural symmetry and stiffness of the molecule does indeed result in robustness of the phase coherence of the molecular orbitals.

When the conductance peaks are measured at higher bias voltage, step-like structures are observed (Fig. 3, right inset). These structures are attributed to contributions from additional levels. Upon reducing the gate voltage, a first current plateau develops when the gg-level enters the bias-window from below. When the levels are pushed up further in energy by ΔE, electrons can now also leave the tube from the lower-lying electron level, leading to a higher current plateau. This lower-lying level is labelled as eg because when it is emptied, the tube is left in an excited state. Current will be blocked again when the gg-level finally leaves the bias-window. From the total peak width, which is set by V_{bias}, we deduce that 12-mV change in V_{gate} results in a change of tube potential of about 1 meV. This conversion can be understood in terms of voltage division: the gate capacitance is one-twelfth of the total capacitance of the tube. The width of the rightmost plateau corresponds to ΔE. On average, we find $\Delta E \approx 0.4$ meV. This value is consistent with the order-of-magnitude estimate $\Delta E \approx 0.6$ meV for a 3-μm-long tube, as mentioned above. This in fact suggests that the coherence extends over the full tube length of 3 μm.

Returning to Fig. 2: the stepwise current increase with increasing V_{bias} may also result from an increasing number of levels within the bias window. These steps are not observed for samples with ropes of tubes. Because of their larger size, they are expected to have a much lower energy separation between levels. A Coulomb staircase[15], which occurs when there is a large difference between the two contact resistances, does not seem to be the origin of the observed steps. For example, the 2-mV width of the step of curve B between $V_{bias} = 1.2$ and 3.2 mV should then be equal to the width of the maximum gap (~6 mV). From Fig. 2 we can also determine the Coulomb charging energy E_c as the width of the maximum gap corresponds to $2(E_c + \Delta E)$. The resulting $E_c \approx 2.6$ meV is in good agreement with an estimate of $E_c \approx 2.5$ meV based on the geometrical self-capacitance of a 3-μm-long tube (3×10^{-17} F). Summing up, the tube appears to have a discrete energy spectrum with an energy level separation of ~0.4 meV, and an extra gap is observed due to a Coulomb energy of ~2.6 meV. Electron transport through discrete electron states has been found previously in systems based on semiconductor two-dimensional electron gases[15] and recently also in a metal system[16].

Single-electron levels will shift in energy upon application of a magnetic field. We measure ΔE as a function of magnetic field B by following the bottom trace of the right inset of Fig. 3 (see Fig. 4). The gg and eg levels appear to move toward each other (situation B in Fig. 4), cross, and separate again (situation C). From the slope of the diagonal line in the contour-plot $d(\Delta E_e)/d(\mu_B B)$, we find a g-factor of 1.9 ± 0.2. This is consistent with magnetic-resonance data[7] and suggests no spin–orbit coupling. It appears that the Zeeman energy is dominant, confirming the expected negligible angular-momentum term. Note that the data do not show splitting of states at $B = 0$ T, as would be expected in the simplest model of level filling and assuming spin degeneracy. This deviation is not yet understood. The plateaux in Fig. 4 appear to be flat over a large range of magnetic field. The tubes thus do not exhibit a magnetoresistance, which would be manifested by a gradual decrease of the peak amplitude as a function of magnetic field. This provides an additional indication that the electronic states are indeed extended and have a one-dimensional nature.

The measurements reported here are, to our knowledge, the first measurements of the electrical transport properties of individual SWNTs. Remarkably, these molecules appear to behave as coherent quantum wires. Considering the strongly one-dimensional nature

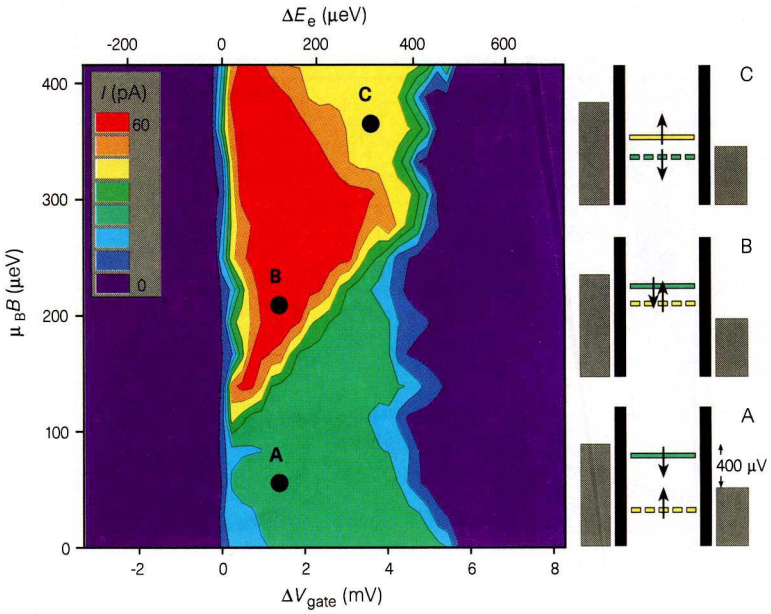

Figure 4 Main figure, current level (see inset colour scale), as a function of $\mu_B B$ and ΔV_{gate} and corresponding relative electrostatic energy ΔE_e, at $V_{bias} = 400$ μV. The magnetic field is applied perpendicular to the tube axis and has a maximum value of 7.5 T. The left current edge has been aligned for all B-values. At low magnetic fields there is a single 'green' current plateau, resulting from the 'green' gg-level with, say, spin down (situation A, right-hand diagrams). The nearest level is the eg-level (yellow) which has spin up and is already outside the bias window. Near 3.5 T (situation B) the two levels appear to have shifted towards each other. They now both contribute to a higher, 'red' current level. At $\Delta V_{gate} \approx 2.5$ mV, the eg-level leaves the bias window. The width of the remaining green plateau corresponds to ΔE. Continuing this trend, the two levels cross and reverse their order (situation C). Now the 'yellow' level has become the gg-level and will leave the bias window last. These observations are consistent with shifting of states due to the Zeeman effect. Note that the difference between the 'green' and 'yellow' current levels implies a different coupling of the two corresponding orbitals to the electrodes.

of the conducting modes in our SWNTs, deviations from Fermi-liquid behaviour may be expected; further analysis and measurements may address this issue. □

Received 3 December 1996; accepted 11 March 1997.

1. Iijima, S. Helical microtubules of graphitic carbon. *Nature* **354,** 56–58 (1991).
2. Dai, H., Wong, E. W. & Lieber, C. M. Probing electrical transport in nanomaterials: conductivity of individual carbon nanotubes. *Science* **272,** 523–526 (1996).
3. Ebbesen, T. W. *et al.* Electrical conductivity of individual carbon nanotubes. *Nature* **382,** 54–56 (1996).
4. Langer, L. *et al.* Quantum transport in a multiwalled carbon nanotube. *Phys. Rev. Lett.* **76,** 479–482 (1996).
5. Bethune, D. S. *et al.* Cobalt-catalysed growth of carbon nanotubes with single-atomic-layer walls. *Nature* **363,** 605–607 (1993).
6. Iijima, S. & Ishihashi, T. Single-shell carbon nanotubes of 1-nm diameter. *Nature* **363,** 603–605 (1993).
7. Thess, A. *et al.* Crystalline ropes of metallic carbon nanotubes. *Science* **273,** 483–487 (1996).
8. Mintmire, J. W., Dunlap, B. I. & White, C. T. Are fullerene tubules metallic? *Phys. Rev. Lett.* **68,** 631–634 (1992).
9. Hamada, N., Sawada, A. & Oshiyama, A. New one-dimensional conductors: graphitic microtubules. *Phys. Rev. Lett.* **68,** 1579–1581 (1992).
10. Saito, R., Fujita, M., Dresselhaus, G. & Dresselhaus, M. S. Electronic structure of chiral graphene tubules. *Appl. Phys. Lett.* **60,** 2204–2206 (1992).
11. Wallace, P. R. The band theory of graphite. *Phys. Rev.* **71,** 622–633 (1947).
12. Dresselhaus, M. S., Dresselhaus, G. & Eklund, P. C. *Science of Fullerenes and Carbon Nanotubes* (Academic, San Diego, 1996).
13. Grabert, H. & Devoret, M. H. (eds) *Single Charge Tunneling* (Plenum, New York, 1992).
14. van Houten, H., Beenhakker, C. W. & Staring, A. A. M. in *Single Charge Tunneling* (eds Grabert, H. & Devoret, M. H.) 167–216 (Plenum, New York, 1992).
15. Geerligs, L. J., Harmans, C. J., P.M. & Kouwenhoven, L. P. (eds) *The Physics of Few-Electron Nanostructures* (North-Holland, Amsterdam, 1993).
16. Ralph, D. C., Black, C. T. & Tinkham, M. Spectroscopic measurements of discrete electronic states in single metal particles. *Phys. Rev. Lett.* **74,** 3241–3244 (1995).

Acknowledgements. We thank L. Kouwenhoven, T. Oosterkamp, R. Groeneveld and Y. Nazarov for discussions and B. van den Enden for technical assistance. The work was supported by the Dutch Foundation for Fundamental Research on Matter (FOM).

Correspondence and requests for materials should be addressed to C.D.

Control of spatial orientation and lifetime of scroll rings in excitable media

Michael Vinson*†, Sergey Mironov*‡, Scott Mulvey* & Arkady Pertsov*

* *Department of Pharmacology, SUNY Health Sciences Center, Syracuse, New York 13210, USA*
† *Department of Physics, Shippensburg University, Shippensburg, Pennsylvania 17257, USA*
‡ *Institute of Cellular Biophysics, Puschino, Moscow Region 142292, Russia*

Excitable media, which range from autocatalytic chemical systems[1–3] to biological cells and tissues[4–7], can maintain organized structures in the form of rotating spiral waves of excitation[8–11]. The dynamics of spiral waves in two-dimensional systems have been shown to be susceptible to control by external fields (such as electric, thermal and optical)[12–14]. In three dimensions, the analogues of spiral waves are scroll waves[9,15,16]. Here we show that an external field—a temperature gradient—can be used to control a particular class of scroll waves called scroll rings. The gradient allows scroll rings to be precisely oriented in space, and their spontaneous shrinkage to be accelerated, decelerated or even reversed (so that the ring expands). The temperature gradient also influences the lifetimes of the scroll rings. We suggest that these dynamics are likely to be generic to other types of field gradients and other excitable media.

The control of three-dimensional (3D) scroll waves is a more complex problem than the control of their two-dimensional analogues, spiral waves. The dynamics of a 3D scroll wave are determined not only by the properties of the excitable medium but also by the shape of the filament (the vortex line about which the wave rotates). Depending on the topology of the filament (for example, open, closed loop, knot), as well as on its curvature, torsion and twist, the dynamics of scroll waves can be significantly different even in the same excitable medium[11,17,18]. This implies that the possibility of controlling scroll waves should strongly depend on a given filament configuration.

Our experiments were carried out in a gel-immobilized Belousov–Zhabotinsky (BZ) reaction[19,20]. Figure 1a is a diagram of a cross-section of a scroll ring, showing the circular axis (filament) about which the wave rotates. Physically, the filament is characterized by zero amplitude of the excitation wave[21]. The wave has the shape of a toroidal scroll, which in this cross-section appears as two counter-rotating spirals. The spatial orientation of the ring is described by the unit vector **S**, normal to the ring plane and with orientation uniquely determined by the sense of rotation of the ring. Figure 1b shows a photograph of an experimental scroll ring in the BZ reaction; Fig. 1c is a reconstruction of its filament, appearing in the projection as a dark ellipse.

Our observations show that there are two effects of an applied temperature gradient: it reorients the plane of the scroll ring so as to align the vector **S** with the gradient vector **g**, and it significantly affects the lifetime of the ring. Once the vectors **S** and **g** become parallel, they remain parallel for the duration of the experiment. (Experiments with initial angles of 0° and 180° showed no reorientation.) The observed relaxation time of the reorientation was found to be long compared to the characteristic rotation period, t_s, of the spiral around the filament.

Figure 2a shows the reorientation of a scroll ring in a gradient of 10 °C cm^{-1}. The filament is shown in lateral projection, and appears as a dark 'dumb-bell' that slowly rotates in the anticlockwise direction. The angles θ between **S** and **g** are shown as filled circles in Fig. 2b. The effect of **g** on the lifetime of the scroll ring can be evaluated by comparing the dynamics of the filament radius (r) in the presence and absence of gradient (Fig. 2b, bottom). In the absence of gradient, the ring shrinks and collapses in 20 minutes (open circles). The gradient prolongs the lifetime of the ring to almost 70 minutes which is about 3.5 times greater than the lifetime in the absence of the field. In a stronger gradient, we found that the

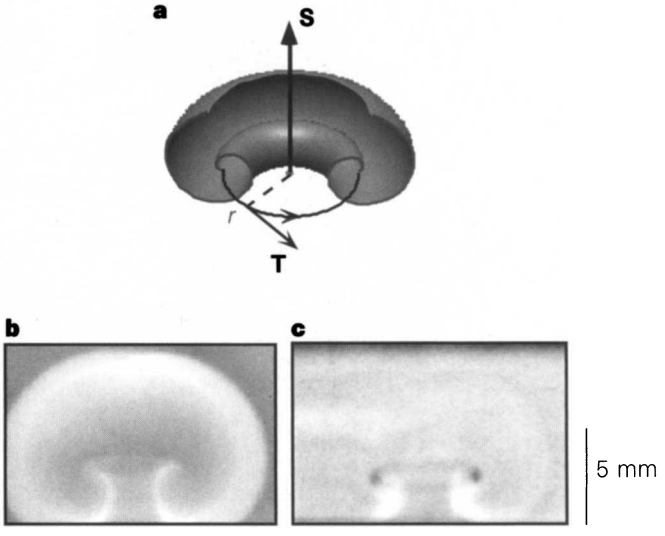

Figure 1 a, Schematic cross-section of a scroll ring. The dark circle of radius r in the centre is the filament of the ring, about which the wave rotates (the spiral on the right rotates clockwise). The unit tangent vector **T** is in the direction of the local angular velocity. The vector **S** is normal to the ring plane, with orientation given by applying the right-hand rule to **T** along the ring. **b**, Photograph of lateral projection of a tilted scroll ring in a gel-immobilized BZ reaction. Excited (oxidized) regions appear lighter. The angle between vector **S** and the vertical axis is 11°. **c**, Photograph of the filament in the same projection. The filament is roughly circular, appearing elliptical in the figure due to the projection.